Applied Thermal Engineering 188 (2021) 116501

Contents lists available at ScienceDirect

Applied Thermal Engineering

journal homepage: www.elsevier.com/locate/ate

Research Paper

Experimental and numerical study of the additive layer manufactured inter-layer channel heat exchanger

Evaldas Greiciunas [a], Duncan Borman [b,*], Jonathan Summers [c], Steve J. Smith [d]

[a] Centre for Doctoral Training in Fluid Dynamics, University of Leeds, Leeds, West Yorkshire, LS2 9JT, United Kingdom
[b] School of Civil Engineering, University of Leeds, Leeds, West Yorkshire, LS2 9JT, United Kingdom
[c] School of Mechanical Engineering, University of Leeds, Leeds, West Yorkshire, LS2 9JT, United Kingdom
[d] BAE Systems, Warton Aerodrome, Warton, Preston PR4 1AX, United Kingdom

ARTICLE INFO

Keywords:
Additive Layer Manufacturing (ALM)
Heat exchangers
Forced convection
Computation Fluid Dynamics (CFD)
Conjugate Heat Transfer (CHT)
Numerical analysis
OpenFOAM

ABSTRACT

In this paper the performance of a recently patented additive layer manufactured (ALM) concept inter-layer heat exchanger (HE) is evaluated experimentally and numerically. Two numerical HE models are developed using the conjugate heat transfer (CHT) methodology. The first is an idealised HE core model, consisting of a single period width HE corrugation section (termed superchannel). The second approach uses a fully detailed HE unit model which resolves the flow and heat transfer inside the complete HE unit. A close agreement was found between the HE unit simulations and the experimentally obtained results, such that the fully detailed HE model could be validated. It was also shown that, a full CHT approach is necessary to accurately evaluate complex inter-layer ALM HE core flow and heat transfer behaviour and can serve as an approach for optimising HE designs. The results also reinforce the occurrence of the inter-layer flow mixing inside the HE core of the same flow streams and allows the mass flow to redistribute inside the HE core which is impossible with the current HE generation geometries. The superchannel model results in a slight over-estimation in heat transfer ($\Delta T \approx 4$ K on average) making the simplified model acceptable as a conservative estimate. Using validated simulations a parametric study was conducted by changing the solid properties of the full CHT HE model to aluminium to investigate the effects of a significantly more conductive material. This resulted in ≈3% higher heat transfer effectiveness (ϵ) of the HE unit. All the simulations were carried out using CFD package OpenFOAM.

1. Introduction

Heat Exchangers (HE) are the devices in which the heat is transferred between two or more fluid streams separated by a solid and are critical components in many industries, such as aerospace, automotive, power generation or chemical & process industry [1]. In high performance applications, such as aerospace and motorsport, the smallest overall HE size is critical since it enables the highest installed component density. This is normally achieved through increasing a number of the heat transfer surfaces (such as fins) and is referred to as compactness in the HE industry. The compactness of a HE is typically measured either using hydraulic diameter (d_h) or the surface area density ($\beta = A_{surface}/V_{flow}$), measuring a ratio of heat transfer area to flow volume. To classify a HE as compact the values for liquids should be at least $d_h \approx 8$ mm and $\beta \approx 400$ m^2/m^3 whilst for gasses they should be at least $d_h \approx 5$ mm and $\beta \approx 700$ m^2/m^3 [2]. Traditionally, the heat transfer surfaces are assembled into HE cores using brazing and connected to fluid streams using headers which are welded on to the HE core [3]. These processes result in HE which are difficult to install when the installation volume is limited.

Additive Layer Manufacturing (ALM) is an exciting branch of manufacturing which offers HE significant advantages over the current methods. They provide a designer with an unprecedented design freedom and a potential for more compact and efficient HE units and expand the traditional heat transfer augmentation techniques such as winglet type vortex generators [4]. ALM has been exploited by many researchers who used numerous ALM techniques for a variety of HE, including Selective Laser Melting (SLM) for heat sinks [5], Direct Metal Laser Sintering (DMLS) [6,7] and Powder Bed Fusion (PBF) for an oil cooler [8]. In the majority of these studies a notable heat transfer improvement is measured, however, it was found to also increase pressure drop which could be partially attributed to a rough surface finish left by the ALM techniques. SLM is a particularly promising ALM method since it results in a more uniform HE structure in contrast to

* Corresponding author.
E-mail address: d.j.borman@leeds.ac.uk (D. Borman).

https://doi.org/10.1016/j.applthermaleng.2020.116501
Received 6 March 2020; Received in revised form 18 December 2020; Accepted 20 December 2020
Available online 12 January 2021

Nomenclature

ALM	Additive Layer Manufacturing
CFD	Computational Fluid Dynamics
DMLS	Direct Metal Laser Sintering
HE	Heat exchanger(s)
PBF	Powder Bed Fusion
SLM	Selective Laser Melting
D_{inlet}	Diameter of the inlet to heat exchanger, m
d_h	hydraulic diameter, m
β	surface area density, $A_{surface}/V_{flow}$, m^2/m^3
u	velocity vector, m/s
ρ	Density, kg/m^3
k	thermal conductivity, W/(mK)
ϵ	heat transfer effectiveness
K	Pressure drop coefficient
p	Pressure, Pa
Δp	Pressure drop, Pa
$Q_{balance}$	Heat balance ($Q_{hot}/Q_{cold} \times 100$)
μ	viscosity, Pa s
μ_t	Turbulent viscosity, Pa s
T	Temperature, K
c_p	specific heat capacity, J/(kgK)
Re_{corrug}	Reynolds number defined as $Re_{corrug} = (\rho U d_h)/\mu$
Re_{inlet}	Reynolds number defined as $Re_{inlet} = (\rho U D_{inlet})/\mu$

brazing or welding. This can provide improved structural integrity and a reduced likelihood of current HE manufacturing flaws, shown in [3]. SLM is also capable of producing solid surfaces at the HE relevant lengthscales (50 μm wall thickness reported in [9]) [10] making it advantageous for HE.

Numerical analysis of compact HE is typically undertaken in two steps: firstly a small section of the HE core is analysed to obtain friction and heat transfer characteristics. These are then implemented in a simplified HE unit model which uses porous media and heat transfer effectiveness models to evaluate macro level flow and heat transfer performance [3,11,12]. In such scenarios, a periodic section of the HE corrugation is often used as introduced by Patankar et al. [13]. This method is computationally cheap and can be used in parametric studies [14,15], however, it has disadvantages for higher Reynolds number predictions [16]. More recently, the trend observed is to model larger sections of HE corrugation, which consist of a finite length HE corrugation channel [3,17,18]. This can provide a better understanding of flow and heat transfer development inside the channel and thus an overall more reliable HE performance prediction. Another emerging trend is to use the Conjugate Heat Transfer (CHT) methodology for compact HE and small sections of both plate-fin [19,20] and tube-fin [21] HE being evaluated. The CHT methodology is undertaken to account the conduction with the fins and is reported to increase accuracy of predictions [20] compared to the traditional single computational domain approaches. A large computational domain for a plate-fin HE was also previously evaluated by the authors [3] in a numerical and experimental study which aimed at accounting the cross-flow heat transfer effects more fully in plate-fin HE applications.

In this study, a previously designed, manufactured [10] and recently patented [22] concept titanium SLM HE is evaluated experimentally and numerically to establish flow resistance and thermal performance characteristics. A fully detailed ALM HE CFD model, employing the CHT methodology is developed and validated using the experimental results. These results are then compared to a more idealised numerical model consisting of a single corrugation period width HE core (superchannel) for heat transfer predictions. Finally, using the validated inter-layer HE unit model a parametric study is undertaken to evaluate the HE performance with aluminium as the HE material to investigate whether any thermal gains are obtained.

Table 1
Properties of the commercially pure titanium provided by outsourced SLM experts.

	Quantity	Uncertainty value	Units
ρ	4510	0.1%	kg/m^3
k	17.7	0.5%	W/(mK)
c_p	500	0.5%	J/(kgK)

2. Experimental approach

An experimental study was conducted to evaluate the concept inter-layer HE which geometry is described in detail in [10]. It was manufactured using SLM out of commercially pure titanium (Fig. 1a) with its relevant properties given in Table 1. This material was selected working in collaboration with the SLM specialist based on a number of factors. Firstly, CpTi has good printability, reliability and repeatability characteristics when used in SLM. Secondly, despite having lower thermal conductivity than materials such as Aluminium or Copper, it is used in the heat transfer industry in heavy duty applications where weaker and softer materials cannot withstand the lifecycle. Also, it was noted that no inter-layer fluid leakages were observed after the build. The concept HE unit consists of four cold and three hot layers which use a counter-flow oriented inter-layer HE corrugation with a mean hydraulic diameter of $d_h = 2.8$ mm (channel height of 5.5 mm, distance between elipses of 2 mm, and ellipse width and length of 2 and 4 mm), uniform wall thickness of 0.5 mm and surface area density of $\beta = 818$ m^2/m^3, shown schematically in Fig. 1b. The surface density of the proposed ALM structure is similar to plate-fin HE and classifies it as compact for both gasses and liquids according to Shah [23]. In contrast to plate-fin corrugations the proposed structure enables the maldistributed flow entering the heat exchanger core to re-distribute across the layers through the inter-layer structure. Maldistributed flow is a common issue in high performance applications such as aerospace and motorsport occurring due to space limitations resulting in restricted header design which leads to non-uniform heat exchanger matrix utilisation. The proposed design in turn has potential for improved utilisation of heat exchanger core volume, enabling either more heat transfer capacity or a smaller heat exchanger for a given application. The HE was tested in an experimental setup as shown in Figs. 1c and 1d with air used as a working fluid for both flow streams. Note, that Fig. 1c shows the uncovered HE unit, which was insulated using Silicon Carbide sheets and experiments were run inside a chamber to further minimise heat loss. To simplify the experiments the hot flow side of the HE was run at a constant Reynolds number of $Re_{inlet} \approx 28760$ ($Re_{inlet} = \rho U D_{inlet}/\mu$). This is equal to $Re_{corrug} \approx 670$ assuming even flow distribution at the HE core inlet ($Re_{corrug} = \rho U d_h/\mu$). The cold fluid stream was varied between $6120 \leq Re_{inlet} \leq 55914$ ($108 \leq Re_{corrug} \leq 980$) with ten separate measurement points recorded.

During the experiments the hot stream air was heated up to $T_{in} \approx 363$ K using a 750 W heater whilst the cold stream was supplied with ambient air (on average $T_{in} \approx 290$ K). The flow on each fluid side was measured using rotameters (KDG Instruments series 2000) which have a +/−2.5% accuracy. Pressure was measured using FC034 pressure transducers, having a +/−0.5% measurement accuracy. Calibrated type K mineral insulated thermocouples were used for measuring the temperature at the inlet and outlet of both fluid streams with a tolerance of ±1.5 K. To ensure repeatability of the experiments, certain points were repeated three times. The thermal experimental uncertainty was measured using heat balance, shown in Fig. 3a and obtained by:

$$Q_{balance} = \frac{Q_{hot}}{Q_{cold}} \times 100 \quad (1)$$

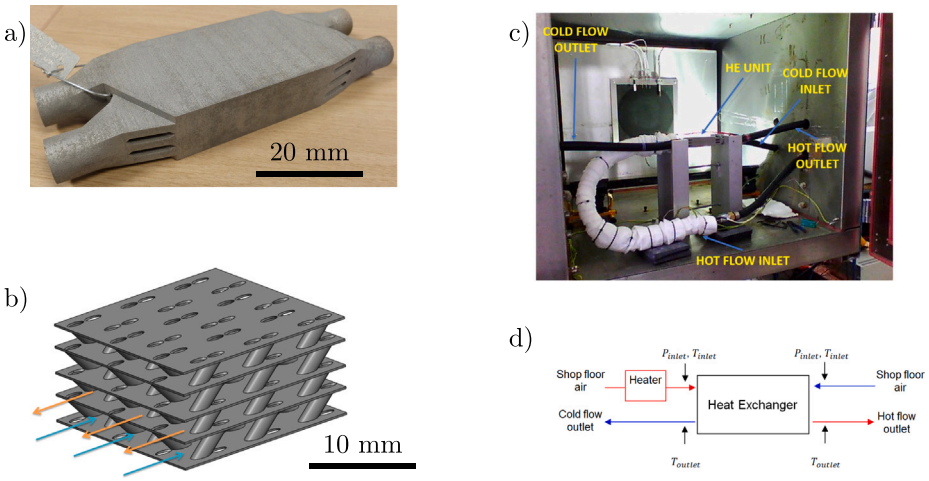

Fig. 1. (a) Manufactured inter-layer HE unit. (b) Schematic of the inter-layer HE core structure. (c) HE unit assembled in the experimental setup. (d) Experimental setup schematic.

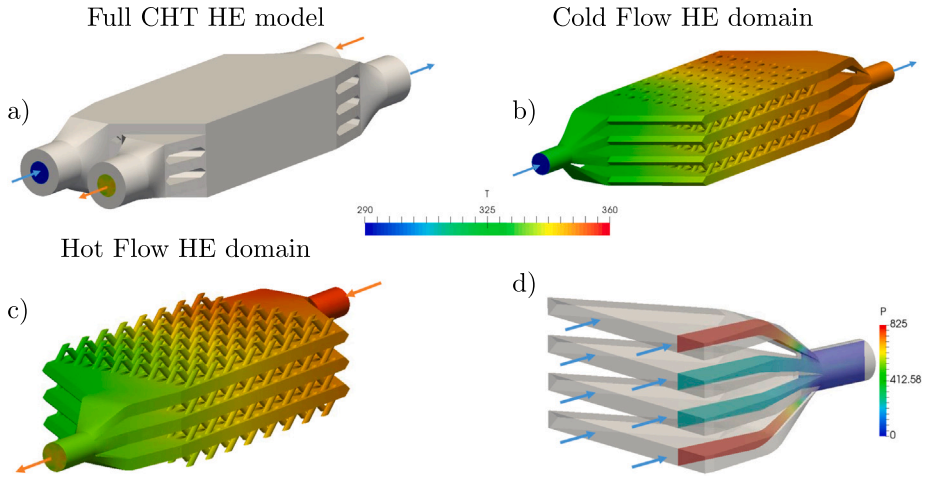

Fig. 2. (a) Complete CHT HE unit model. (b) Cold HE unit domain. (c) Hot HE unit domain. (d) Outlet HE header model for the cold flow.

where Q_{hot} is the heat emitted by the hot stream and Q_{cold} is the heat absorbed by the cold stream. This formulation means that a scenario in which the heat balance is below 100 (more heat absorbed than emitted) is not physical since some heat loss to the environment is expected despite insulating the HE. It should also be noted that the error bars placed on the measured heat balance (Fig. 3a) show the maximum possible error due to the measurement accuracy of the experimental equipment described above. However, this level of error is unlikely as indicated by the repeated experimental points in Fig. 3a, where on average the fluctuation between the experimental heat balance is <5%. This confirms a good repeatability level of the experiments which were completed over a time span of two weeks. It should be noted that the highest repeatability error was found at the lower Reynolds numbers, which likely arises from difficulty measuring the very small mass flow in the test rig. The pressure for both fluids was measured at the inlet to each HE stream. To calculate the pressure drop this pressure was subtracted from the atmospheric pressure measured during the experiments, shown in Fig. 3b. This measurement technique resulted in the need to apply experimental correction since due to the setup, a pressure drop occurs as a result of the sudden expansion in the pipe diameter at the outlet section of the experimental rig. It occurs at a location where the flow exits the HE header (D_{in} = 13 mm) and enters the rubber ducting connected on the outer diameter of the HE header surface (D_{out} = 27 mm) (Figs. 1a and 1c). The contribution of this additional pressure loss was taken into account by using the well established analytical formula for a head loss in a pipe, taken from White [24]:

$$\Delta p = K\frac{\rho U^2}{2} \tag{2}$$

where U was taken as a mean velocity at the inlet to the HE (worked out from the mass flow) and K = 0.6 was selected based on [24]. Note, that the K coefficient does not account for the slight turn in the outlet tubing, leading to a potential slight under-estimation of the pressure drop in that section. The corrected pressure drop data in Fig. 3b and shows the increasing influence of the pressure drop in the pipe expansion section compared to the pressure drop in the HE unit and it should be noted for any future experimental setup design.

3. Numerical solution methodology

Numerical simulations undertaken in this study are an extension of the single fluid domain analysis undertaken in [10]. In this study, CFD simulations of the inter-layer ALM HE were undertaken with the CFD code OpenFOAM using steady-state incompressible continuity of mass, momentum and energy equations for the fluid domain [25]:

$$\nabla \cdot \mathbf{u} = 0 \tag{3}$$

$$\rho_f(\mathbf{u}\cdot\nabla)\mathbf{u} = -\nabla p + \mu_{eff}\nabla^2\mathbf{u} \tag{4}$$

$$\mathbf{u}\cdot\nabla T_f = \alpha_{eff}\nabla^2 T_f \tag{5}$$

Table 2
Discretisation schemes used for the simulations.

Term	Discretisation scheme
Gradient (∇)	Gauss linear
Laplacian (∇^2)	Gauss linear corrected
div(phi,U)	Gauss linearUpwind grad(U)
div(phi,h)	Gauss linearUpwind grad(h)
div(phi,k)	Gauss upwind
div(phi,omega)	Gauss upwind

Table 3
Mesh data of the CHT ALM HE unit model compared to the experimentally measured results.

Mesh	No of Cells	Cold side		Hot side	
		ΔP, Pa	ΔT, K	ΔP, Pa	ΔT, K
Coarse	4.4×10^6	59	60.2	998	12.3
Medium	25.2×10^6	68	63.2	1092	13.1
Fine	55.6×10^6	73	63.0	1105	12.9
Test	N/A	62	58	1070	12.9

where **u** — mean RANS velocity vector, p — fluid pressure, T_f — fluid temperature, ρ_f — fluid density. $\mu_{eff} = \mu + \mu_t$, where μ_t is the dynamic turbulent viscosity and calculated based on the $k-\omega\ SST$ turbulence model [26] used in this paper and $\alpha_{eff} = \alpha_f + \mu_t/(\rho Pr_t)$, where $\alpha_f = k_f/(\rho_f C p_f)$ and Pr_t is the turbulent Prandtl number taken to be 0.85 in RANS simulations. Note that $y+$ adaptive wall treatment was used. All the predictions in this article used smooth no-slip wall assumption (since surface roughness data of the prototype was not available) and the CHT formulation, thus, included resolving heat transfer in the solid region, separating the hot and cold HE flows. This was undertaken solving the heat conduction equation:

$$\alpha_s \nabla^2 T_s = 0. \tag{6}$$

The steady-state assumption was maintained throughout all the simulations as it has been previously shown to produce accurate predictions of pressure drop and temperature change in studies [3,10] for the Reynolds number range at which the HE unit was experimentally tested. It is, however, acknowledged that there could be unsteady flow features as indicated in [16] together with experimental [27,28] and numerical studies [4,17,29] which provide insight into these transient effects. The effect of the unsteady flow features is considered small for the HE of this study. The simulations were discretised using two levels of approximation provided in Table 2 whilst the meshing was completed using a combination of the inbuilt `blockMesh` and `snappyHexMesh` tools within OpenFOAM, ensuring that default mesh quality conditions (non-orthogonality, skewness, aspect ratio) in OpenFOAM were met.

3.1. Computational domains and grid independence

In this section the fully detailed HE model including CHT (cold and hot fluid domains separated by a solid) is undertaken (Figs. 2a, 2b and 2c). The fully detailed model approach produces results in good agreement with experiments and enables the observation and evaluation of the complex flow through the inter-layer HE corrugation. This approach is contrary to the normal practice of simplifying the flow and heat transfer inside the HE unit with porous media and heat transfer effectiveness models [10]. To check the accuracy of the solutions a range of HE unit meshes were created and compared to the first experimental test point (Table 3) using second order dominant discretisation (Table 2). Medium and fine meshes show both convergence in terms of temperature and pressure between the solutions. Additionally an acceptable agreement to the experimental data is also shown (note that potential experimental inaccuracies are more likely for the first point (Fig. 1a), driven by low mass flow rate on the cold side). Fine resolution HE unit mesh was selected for further simulations — further increase in mesh resolution was treated as an overly high computational cost.

The superchannel model (Fig. 4a) is the second HE core model used in this study and consists of one corrugation period width slice of the HE core following the methodology in [10]. It produces idealised HE core thermal performance and pressure drop predictions since the model does not take into account the maldistributed flow as it enters the HE core. The meshing controls of from the HE unit model were used for the smaller superchannel model which also uses the CHT methodology. This ensures comparability between the superchannel and HE unit models through maintaining the same mesh resolution. To estimate the HE unit flow resistance together with the superchannel model thermal predictions, the cold HE side outlet header was modelled (Fig. 2d). Again, the same meshing controls as for the HE unit model were applied, which maintains the solution similarity with the other two models. This is done since [10] showed that the pressure drop for this HE is dominated by the outlet HE header effects. This two model approach allows a computationally cheaper estimate of the HE unit performance, however, it is also important to understand the inaccuracy it produces which is studied in the next section.

4. Results

4.1. Validation of the numerical results with the experiments

In this section the results of the two numerical HE models are presented and compared to the experimental work. Firstly, the HE unit pressure drop is compared in Fig. 4b and it can be seen clearly that both full HE unit models predict pressure drop very close to the experimentally measured values. Interestingly, the pressure drop of both discretisation accuracy approaches produce almost an identical response. This is in contrast to the previous findings in [16] where a two dimensional sinusoidal corrugation was evaluated and led to a higher pressure drop. However, in the current study the pressure drop is measured at the HE unit level and was shown to be highly dominated by the outlet header effects [10] which could have reduced the importance of more accurate discretisations.

This can be further seen when looking at the cold flow outlet HE header (Fig. 2d) pressure drop in Fig. 4b. This simplified model uses a uniform velocity inlet to the domain and in turn directs more mass flow through the outer layers of the HE core where the passage of the flow is more difficult. This in turn leads to an increased pressure drop overprediction (up to 60%) using the outlet HE header alone (further highlighting the pressure drop inefficiencies inside the outlet header design). It should be noted though that this is a proof of concept HE, and the design is not claimed to be an optimum at this stage. Additionally, as this reduced complexity model provides a significant computational saving, it is considered to be a potentially useful option for a conservative pressure drop estimate, especially in the more optimised HE header design cases.

Mass flow redistribution inside the HE core (Figs. 5a–5b) is another area of interest and is critical for evaluating the performance of the concept inter-layer corrugation. Here the HE core layers are numbered 1–4 bottom to top for the cold HE side (Fig. 2a) and 1–3 bottom to top for the hot HE side (Fig. 2c). For the cold HE side (Fig. 5a), the performance is very similar to the results obtained in the previous numerical study [10] where it was found that almost double the initial mass flow into the outer HE core layers is absorbed (Layers 1 and 4) across the range of $108 \leq Re \leq 979$. A similar trend is also observed on the hot side of the HE (Fig. 5b) which was kept almost at a constant flow rate during experiments. In this case the flow direction is the opposite (as the HE is counter flow) and there are three hot HE core layers which are surrounded by the cold flow. Thus, in Fig. 5b the mass flow redistribution between the layers can be observed in Layers 1 and 3 reaching almost double the initial entrained mass flow. This

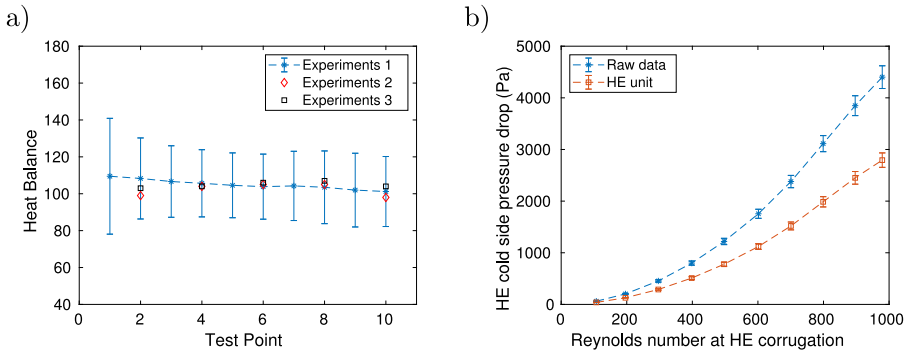

Fig. 3. (a) Heat balance of the HE experiments (b) Cold HE side pressure drop. Please note that error bars on both graphs show the maximum possible experimental uncertainty, explained in Section 2.

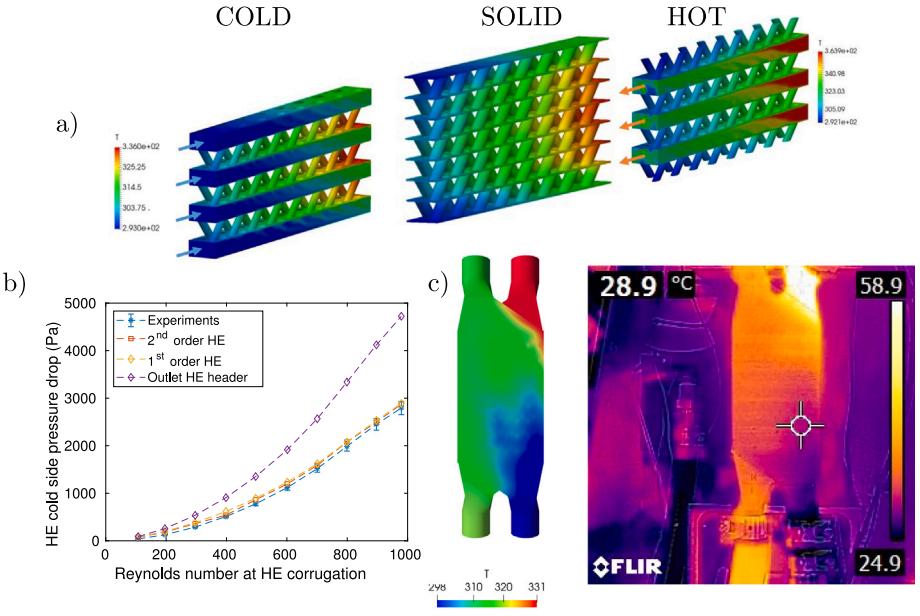

Fig. 4. (a) Break-down of the superchannel HE unit model computational domains. (b) Comparison of the cold side HE overall experimental pressure drop and the different numerical models. (c) Qualitative thermal camera temperature contours for comparison of experiments and numerical simulations at $Re_{cold} = 979$ and $Re_{hot} = 679$.

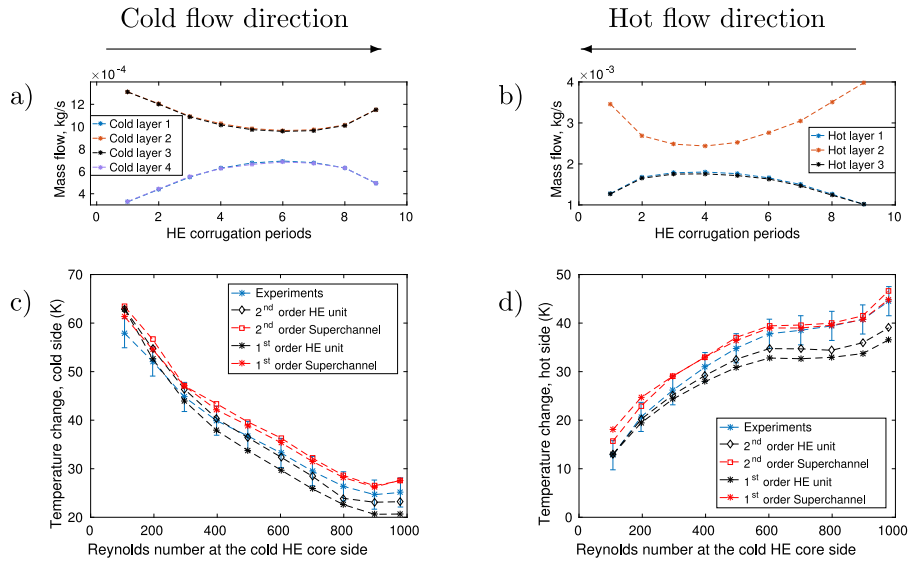

Fig. 5. (a) Mass flow distribution through the cold side HE corrugation periods at $Re_{cold} = 296$ (b) (a) Mass flow distribution through the hot side HE corrugation periods at $Re_{hot} = 667$ (c) Temperature change ΔT, K of the cold side of the HE across experimental points (d) Temperature change ΔT, K of the hot side of the HE across hot side experimental points.

would not have been possible on both sides of the HE without the inter-layer passages. It reinforces the potential advantages of the inter-layer channels (previously studied in [10]).

In terms of the thermal performance it is firstly compared qualitatively in 4c where during the last experimental point the thermal HE insulation was removed and the thermal image was taken using a FLIR thermal camera. This is not a fully accurate experimental result due to the thermal leakage to the environment and relatively low image resolution of the camera (640 × 480). However, the image provides a good indication of heat transfer distribution across the HE unit and allows to directly compare it with the solid HE unit computational domain results at the same experimental point (in terms of showing the hot and cold regions of the HE unit which should be minimised to achieve better overall HE unit efficiency). Overall, close agreement can be seen between the numerical and experimental results which reinforces confidence in the numerical simulation. Further comparison of the thermal results is shown in Figs. 5c and 5d. Here both the superchannel and the full HE unit models are compared across the experimental dataset for cold and hot HE sides (the cold flow was varied $108 \leq Re_{\text{corrug cold}} \leq 979$ whilst the hot flow was maintained at $Re_{\text{corrug hot}} \approx 670$). Several interesting trends can be observed and are discussed below.

Both models (HE unit and superchannel) were discretised to both first and second order accuracy which revealed an interesting difference between them. For the HE unit predictions higher accuracy discretisation led to a larger thermal prediction (up to $T \approx 2.5$ K at the last experimental point) with increasing cold side flow rate. This difference also starts to become noticeable from $300 \approx Re_{\text{corrug cold}} \approx 400$, close to the previously suspected onset of the transitional flow occurring in HEs [3,10,16]. The first order dominant discretisation was shown previously [16] to omit this flow regime occurring, producing a steady-state response. This onset of the transitional flow is also thought to lead to increasing disagreement between experiments and HE unit predictions in terms of the overall ΔT on both fluid sides which remains within the experimental error bars for the cold side and just outside ($T \approx 2$ K) from the error bars on the hot side. The challenge of measuring the low experimental mass flow is also a potential secondary reason why the temperature change might had a lower predicted value. This can be a factor on the hot side especially as the flow measurement was calibrated at room conditions.

In contrast, no difference is observed when comparing the predictions of the first and second order accuracy dominant discretisations using the superchannel model (Figs. 5). This is an unexpected result, however, it perhaps indicates that the effect of the discretisation may only become significant in more complex flow scenarios (e.g the full HE unit case discussed above). The unsteady flow occurrence is thought to also have a smaller effect on this particular HE within the Reynolds numbers tested. This is based on the previous results [10] where it was shown that at least to $Re_{corrug} = 1000$ both steady state and transient predictions lead to very similar results of pressure drop and temperature change. The thermal predictions using the superchannel model are also constantly higher than with the HE unit model and this increases at higher Reynolds number. This is expected and was also observed in the previous study [10] and occurs because the superchannel model is and does not take into account the complex inlet HE header effects. However, superchannel is seem to be a very useful HE core model since it leads to significant computational cost reduction. Additionally, the superchannel model shows the potential of the HE core if it was equipped with more efficient headers (this in theory shows that an additional 5 K could be lost/gained by the cold/hot HE sides respectively at the highest Reynolds number).

To summarise, the CFD is in a good agreement with the experimental results for pressure drops across the Reynolds number range tested. For the temperature change the agreement on both cold and hot HE sides is good, especially taking into account both experimental and numerical challenges for resolving the flow in the transitional Reynolds regime. Both first and second order dominant discretisation schemes can be applied for analysing the HE, but it should be kept in mind that at the higher Reynolds numbers the first order approach is likely to lead to some solution inaccuracies. First order dominant discretisation schemes could be useful for estimating flow and heat transfer through complicated HE corrugations or when used for large computational domains where the faster convergence is advantageous from a pragmatic perspective.

Table 4
Relevant properties of the AlSi10Mg which could be used to manufacture the prototype HE, taken from EOS (SLM manufacturer) website [30].

	Quantity	Units
ρ	2670	kg/m^3
k	173	W/(mK)
c_p	890	J/(kgK)

Table 5
Thermal diffusivities of the Aluminium and Titanium used in the parametric study.

	α, [m^2/s]
AlSi10Mg	7.28×10^{-5}
CpTi	3.92×10^{-7}

4.2. Effect of higher conductivity material for the heat transfer efficiency

Achieving good model agreement with the experimental data provided confidence to carry out a parametric study of the HE unit. One particular concern raised during both manufacture and testing was the usage of commercially pure Titanium due to its non-optimal thermal properties (Table 1). Thus, it was decided to study a scenario in which the HE unit would be manufactured using an Aluminium powder (AlSi10Mg). Its properties were taken from one of the HE manufacturers and summarised in Table 4. It also should be noted that the thermal properties of the Aluminium ALM powder are also very similar to ones of conventional HE aluminium [3] which shows potential of the technology for the next generation HE. Comparing the commercially pure titanium (Table 1) and Aluminium (Table 4), it can be easily observed that the Aluminium has significantly higher potential for heat transfer which can be compared using the material thermal diffusivity [31]:

$$\alpha = \frac{k}{\rho c_p}, \left[\frac{\text{m}^2}{\text{s}}\right] \tag{7}$$

with the results provided in Table 5. It can be clearly seen that the overall potential for the Aluminium to transfer more heat is more than of an order higher and one could intuitively expect significantly more efficient heat transfer. Thus, the material properties were implemented into the superchannel and HE unit models to evaluate whether using Aluminium would enhance the heat transfer for the HE unit. The simulations in this case were completed using the dominant second order accuracy for both Aluminium and Titanium (Table 2). The results were compared using heat transfer effectiveness formulations for both hot and cold HE sides [31,32]:

$$\epsilon = \frac{\text{Actual heat transfer}}{\text{Maximum possible heat transfer}}, \tag{8}$$

which for the two HE sides becomes:

$$\epsilon_{cold} = \frac{C_{cold}(T_{\text{out cold}} - T_{\text{in cold}})}{C_{min}(T_{\text{in hot}} - T_{\text{in cold}})} \tag{9}$$

$$\epsilon_{hot} = \frac{C_{hot}(T_{\text{in hot}} - T_{\text{out hot}})}{C_{min}(T_{\text{in hot}} - T_{\text{in cold}})} \tag{10}$$

where $C_{cold} = \dot{m}_{cold} c_p$, $C_{hot} = \dot{m}_{hot} c_p$ and $C_{min} = \min(C_{cold}, C_{hot})$. The two expressions (Eq. (10)) enable evaluation of the heat transfer efficiency for both models with the data shown in Fig. 6. Contrary to the original expectation, only a relatively low increase in the heat

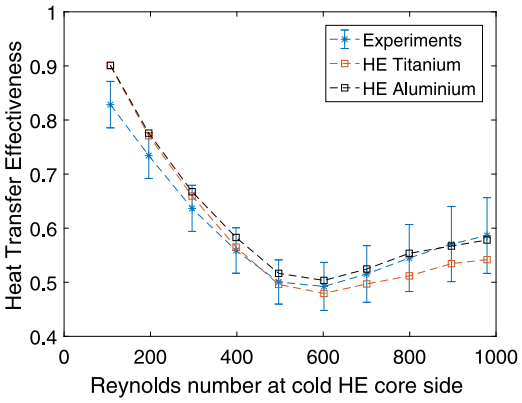

Fig. 6. Heat transfer effectiveness of the HE comparing the effect of titanium and aluminium used as a solid material.

transfer effectiveness is observed (on average a 3% increase). However, it is thought that this can be explained by the low wall thickness used for the HE unit (uniform 0.5 mm in both HE header and HE core) which in turns reduces the importance of the separating material. Furthermore, the inter-layer heat exchanger has no secondary heat transfer surfaces (fins) which makes the heat transfer more efficient and the role of highly conductive material less critical. The supporting evidence for this can be found in heat exchanger literature such as Shah and Sekulic [31] and Kays and London [32]. The example HE sizing calculations using the analytical $NTU-\epsilon$ HE model in Kays and London [32] does not even take into account the thermal primary heat transfer surface solid resistance into account and assumed it negligible. It is only used in the later literature, however, described as a minor diffusive loss as in Shah and Sekulic [31] and they also emphasise that the role of the primary surface conduction becomes significant only in cases of low conductivity materials (e.g. ceramics and plastics) or high wall thickness. However, in both books [31,32] the analytical HE models do take into account the fin efficiency (for the concept HE design it is unity). Thus, it could potentially be expected that for current generation HE, such as plate-fin HE, change in material would make a more significant difference due to the dominance of the secondary heat transfer surfaces, especially for thicker surfaces. Additionally, in [31] it is stressed that the heat transfer resistance in the fluid film is typically a dominant force. Such results were observed in an study by Luo and Roetzel [33] where performance of an aluminium and stainless steel plate-fin HE was modelled and found that conduction played a much smaller role in the case of Aluminium finned structure whilst for the stainless steel structure (thermal conductivity is comparable to titanium) stronger fin conduction resistance effect is reported. No fins are present in the proposed inter-layer HE, making it an overall inherently more efficient HE (already in addition to the counter-flow orientation). Furthermore, elimination of fins should also minimise the transient heat transfer effects, occurring due to a change in flow conditions.

However, the findings of Luo and Roetzel [33] also provide a reason why some improvement in heat transfer effectiveness is found and is at ≈3%. In the case of the HE unit (Fig. 2a–2c) — the flow entering both hot and cold flow HE core sections is maldistributed. This creates sections inside the HE core where the heat transfer is not optimised (e.g. in regions where flow recirculates). This in turn leads to higher importance of efficient lateral solid conduction for those regions, making Aluminium HE more efficient.

5. Conclusions

The recently patented concept titanium inter-layer HE, manufactured using the SLM method, was evaluated experimentally producing a comprehensive dataset and modelled using CFD. It should be noted that this HE is an initial concept and it is not aimed to be an optimised design for a specific application. Two HE models were developed using a CHT methodology: firstly, a fully detailed HE unit model was developed in order to capture the complex flow and heat transfer in full detail. The second model used the simplified single corrugation width HE core model (termed superchannel) for thermal predictions and the outlet HE header to account for the pressure drop contribution. The main findings of the study are:

- A very close agreement is found between the HE unit model and the experiments in terms of the pressure drop performance across Reynolds number range. In terms of the thermal performance, a good agreement was found between the HE unit model and the experiments with most of the prediction points lying within the experimental error bounds. The results provide a validation of the full CHT HE numerical model.
- The superchannel model consistently provided slightly higher thermal transfer rates in terms of ΔT since it provides an idealised heat transfer scenario where no maldistribution inside the inlet HE header occurs. However, the superchannel model is still valuable since it shows the maximum thermal efficiency this HE core could obtain and is significantly computationally cheaper than the complete HE model. Simulating the outlet HE header separately produced an increasingly higher pressure drop compared to the experiments (up to $\approx$ 60%). However, since simulating the HE header separately is significantly faster computationally and over the lifetime of the HE, its pressure drop of the HE is expected to increase significantly ([34–36] reported fouling related pressure drop increase up to 200%), the separate HE header model can still be used as a conservative pressure drop estimate.
- A study was conducted by altering the solid domain from titanium to aluminium to evaluate the HE performance using a more thermally conductive material. On average, approximately a 3% increase in heat transfer effectiveness was observed. The thermal conduction was found to have a smaller influence than originally expected and is thought to relate to: firstly, the proposed inter-layer HE corrugation eliminates secondary heat transfer surfaces (fins) which reduces the role of solid conduction. Secondly, the low uniform (0.5 mm) overall wall thickness, which further minimises the role of solid conduction.

Declaration of competing interest

The authors declare that they have no known competing financial interests or personal relationships that could have appeared to influence the work reported in this paper.

Acknowledgements

The authors would like to thank the primary sponsor BAE Systems for their support. This work also was supported by the Engineering and Physical Sciences Research Council (EPSRC) Centre for Doctoral Training in Fluid Dynamics at the University of Leeds, United Kingdom under Grant No. EP/L01615X/1.

References

[1] W.M. Rohsenow, J.P. Hartnett, Y.I. Cho, et al., Handbook of Heat Transfer, vol. 3, McGraw-Hill, New York, 1998.
[2] R.K. Shah, Compact Heat Exchanger Surface Selection, Optimization, and Computer Aided Thermal Design, Hemishpere, New York, 1983.
[3] E. Greiciunas, D. Borman, J. Summers, S. Steve J., A multi-scale conjugate heat transfer modelling approach for corrugated heat exchangers, Int. J. Heat Mass Transfer 139 (2019) 928–937.
[4] A. Sinha, H. Chattopadhyay, A.K. Iyengar, G. Biswas, Enhancement of heat transfer in a fin-tube heat exchanger using rectangular winglet type vortex generators, Int. J. Heat Mass Transfer 101 (2016) 667–681.

[5] M. Wong, I. Owen, C. Sutcliffe, A. Puri, Convective heat transfer and pressure losses across novel heat sinks fabricated by selective laser melting, Int. J. Heat Mass Transfer 52 (1–2) (2009) 281–288.
[6] X. Zhang, R. Tiwari, A.H. Shooshtari, M.M. Ohadi, An additively manufactured metallic manifold-microchannel heat exchanger for high temperature applications, Appl. Therm. Eng. 143 (2018) 899–908.
[7] M.A. Arie, A.H. Shooshtari, M.M. Ohadi, Experimental characterization of an additively manufactured heat exchanger for dry cooling of power plants, Appl. Therm. Eng. 129 (2018) 187–198.
[8] D. Saltzman, M. Bichnevicius, S. Lynch, T.W. Simpson, E.W. Reutzel, C. Dickman, R. Martukanitz, Design and evaluation of an additively manufactured aircraft heat exchanger, Appl. Therm. Eng. 138 (2018) 254–263.
[9] I. Yadroitsev, P. Bertrand, I. Smurov, Parametric analysis of the selective laser melting process, Appl. Surf. Sci. 253 (19) (2007) 8064–8069.
[10] E. Greiciunas, D. Borman, J. Summers, S.J. Smith, A numerical evaluation of next generation additive layer manufactured inter-layer channel heat exchanger, Appl. Therm. Eng. 162 (2019) 114304.
[11] L.S. Ismail, C. Ranganayakulu, R.K. Shah, Numerical study of flow patterns of compact plate-fin heat exchangers and generation of design data for offset and wavy fins, Int. J. Heat Mass Transfer 52 (17) (2009) 3972–3983.
[12] A.M. Hayes, J.A. Khan, A.H. Shaaban, I.G. Spearing, The thermal modeling of a matrix heat exchanger using a porous medium and the thermal non-equilibrium model, Int. J. Therm. Sci. 47 (10) (2008) 1306–1315.
[13] S. Patankar, C. Liu, E. Sparrow, Fully developed flow and heat transfer in ducts having streamwise-periodic variations of cross-sectional area, J. Heat Transfer 99 (2) (1977) 180–186.
[14] J. Zhang, J. Kundu, R.M. Manglik, Effect of fin waviness and spacing on the lateral vortex structure and laminar heat transfer in wavy-plate-fin cores, Int. J. Heat Mass Transfer 47 (8) (2004) 1719–1730.
[15] K. Kelkar, S. Patankar, Numerical prediction of flow and heat transfer in a parallel plate channel with staggered fins, J. Heat Transfer 109 (1) (1987) 25–30.
[16] E. Greiciunas, D. Borman, J. Summers, Unsteady flow modelling in plate-fin heat exchanger channels, in: ASME 2017 Summer Heat Transfer Conference, American Society of Mechanical Engineers, 2017.
[17] Z. Zheng, D.F. Fletcher, B.S. Haynes, Transient laminar heat transfer simulations in periodic zigzag channels, Int. J. Heat Mass Transfer 71 (2014) 758–768.
[18] Z. Dai, D.F. Fletcher, B.S. Haynes, Impact of tortuous geometry on laminar flow heat transfer in microchannels, Int. J. Heat Mass Transfer 83 (2015) 382–398.
[19] M. Ferrero, A. Scattina, E. Chiavazzo, F. Carena, D. Perocchio, M. Roberti, G.T. Rivalta, P. Asinari, Louver finned heat exchangers for automotive sector: Numerical simulations of heat transfer and flow resistance coping with industrial constraints, J. Heat Transfer 135 (12) (2013) 121801.
[20] T. Perrotin, D. Clodic, Thermal-hydraulic CFD study in louvered fin-and-flat-tube heat exchangers, Int. J. Refrig. 27 (4) (2004) 422–432.
[21] A.A. Bhuiyan, M.R. Amin, A.S. Islam, Three-dimensional performance analysis of plain fin tube heat exchangers in transitional regime, Appl. Therm. Eng. 50 (1) (2013) 445–454.
[22] E. Greiciunas, D. Borman, J. Summers, S. Smith, Heat exchanger, WO2019171079A1, URL: https://patents.google.com/patent/WO2019171079A1.
[23] R.K. Shah, Classification of heat exchangers, in: S. Kakac, A.E. Bergles, F. Mayinger (Eds.), Heat Exchangers: Thermal-Hydraulic Fundamentals and Design, Hemisphere Publishing, Washington, DC, 1981, pp. 9–46.
[24] F. M.White, Chapter 6 viscous flow in ducts, in: Fluid Dynamics, fifth ed., WCB McGraw Hill, PO Box 182605, Columbus OH 43218-2605 USA, 2003.
[25] S. Chandrasekhar, Hydrodynamic and hydromagnetic stability, Courier Corporation, 2013.
[26] F.R. Menter, M. Kuntz, R. Langtry, Ten years of industrial experience with the SST turbulence model, Turb. Heat Mass Transf. 4 (1) (2003) 625–632.
[27] T. Rush, T. Newell, A. Jacobi, An experimental study of flow and heat transfer in sinusoidal wavy passages, Int. J. Heat Mass Transf. 42 (9) (1999) 1541–1553.
[28] T. Nishimura, K. Yano, T. Yoshino, Y. Kawamura, Occurrence and structure of taylor-goertler vortices induced in two-dimensional wavy channels for steady flow, J. Chem. Eng. Japan 23 (6) (1990) 697–703.
[29] M. Hiramatsu, T. Ishimaru, T. Ohkouchi, Numerical analysis of innerfins for intercoolers, JSME Int. J. Ser. 2 35 (3) (1992) 406–412.
[30] EOS, EOS metal materials for additive manufacturing, https://www.eos.info/material-m.
[31] R.K. Shah, D.P. Sekulic, Fundamentals of Heat Exchanger Design, John Wiley & Sons, 2003.
[32] W.M. Kays, A.L. London, Compact Heat Exchangers, McGraw-Hill, 1964.
[33] X. Luo, W. Roetzel, The single-blow transient testing technique for plate–fin heat exchangers, Int. J. Heat Mass Transfer 44 (19) (2001) 3745–3753.
[34] I.H. Bell, E.A. Groll, Air-side particulate fouling of microchannel heat exchangers: experimental comparison of air-side pressure drop and heat transfer with plate-fin heat exchanger, Appl. Therm. Eng. 31 (5) (2011) 742–749.
[35] R. Lankinen, J. Suihkonen, P. Sarkomaa, The effect of air side fouling on thermal-hydraulic characteristics of a compact heat exchanger, Int. J. Energy Res. 27 (4) (2003) 349–361.
[36] R. Haghighi-Khoshkhoo, F. McCluskey, Air-side fouling of compact heat exchangers for discrete particle size ranges, Heat Transf. Eng. 28 (1) (2007) 58–64.